The Mechanism of Ion Conduction and Dynamics in tris(*N,N*-Dimethyl-formamide)perchloratosodium Solid Electrolytes

Prabhat Prakash, [†,‡] Ardhra Shylendran, [‡] Birane Fall, [§] Michael J. Zdilla, [§*] Stephanie L. Wunder, [§*] Arun Venkatnathan. [‡*]

[†] Materials Science and Engineering, Indian Institute of Technology Gandhinagar, Gujarat 382355, India.

[‡] Department of Chemistry and Centre for Energy Science, Indian Institute of Science Education and Research Pune, Dr. Homi Bhabha Road, Pashan, Pune 411008, India.

[§] Department of Chemistry, Temple University, 1901 N. 13th St., Philadelphia, PA 19086, USA.

Batteries, electrolytes, sodium-ion batteries, ionic conductivity.

ABSTRACT: $(DMF)_3NaClO_4$ is a soft-solid cocrystalline electrolyte with channels of Na^+ ions, which can be reversibly converted to a less conductive form $(DMF)_2NaClO_4$ by application of pressure or heat, leading to a melt- or press-castable electrolyte. Molecular dynamics simulations performed on the 3:1 stoichiometry suggest that Na^+ ions conduct via a one-dimensional channel, which is supported by van-Hove autocorrelation function analysis. The simulations show that the transference number for Na^+ ions is 0.43 at room temperature and exceeds 0.5 at higher temperatures in the molten mixture. The calculated activation energy for diffusion of Na^+ ions from MD simulations is 45 kJ-mol^{-1}. The minimum energy path of Na^+ ion migration in 3:1 crystal is assessed using periodic density functional theory calculations, which provides a barrier of 33 kJ-mol^{-1} for Na^+ ion conduction, in reasonable agreement with the experimental value of 25 kJ-mol^{-1}. The motion of Na^+ ions during conduction is vacancy-driven, as the presence of a vacancy site enables jump events for Na^+ ions. The activation energy is the penalty for a sodium ion to leave the octahedrally coordinated DMF ligand field via a transition state where only three molecules of DMF form a 3-O-Na trigonal planar geometry, with no involvement of the ClO_4^- in the coordination sphere of the transition state. In contrast, the calculated activation energy barrier for the 2:1 stoichiometry is higher ($E_{a,DFT}$ = 43 kJ-mol^{-1}, $E_{a,exp}$ = 49 kJ-mol^{-1}) due at least in part to the partial coordination of strongly binding perchlorate anions with Na^+ ions in the transition state.

Introduction

Solid state electrolytes are key components for development of thermally and mechanically stable metal-ion batteries[1,2]. The use of sodium in rechargeable batteries will be cost effective due to its abundance, and enduring as a substitute for lithium-ion batteries (LIB) in applications that can tolerate lower energy density batteries[3]. A pervasive problem with both technologies is flammability of the liquid organic electrolyte, which has led to explosion and fire[4,5]. In the exploration of potentially safer electrolytes for sodium ion batteries (SIBs), solid electrolytes (sodium superionic conductors (NASICON)[6,7], ceramics[8], polymers and their composites), and non-flammable liquid electrolytes (e.g. non-flammable organic solvents[9], ionic liquids[10]) have been explored. Soft solids such as polymers have poor ionic conductivity but are good electronic insulators. Hard solids like ceramics and NASICONs show excellent mechanical and thermal stability but are brittle and exhibit poor ionic conductivity in pressed pellets compared to liquid electrolytes.[6,11,12] Despite reports on certain ceramics which demonstrate excellent ionic conductivities in sintered pellets[11,13], high resistance in the contact layers formed between the grains leads to poor intergranular (grain boundary) and interfacial (electrode/electrolyte) conductivity[14,15]. Ion migration in such materials occurs via complex molecular mechanisms including interstitial ion displacements, defect jumps and superionic diffusion[16–19]. In several hard-solid SIB/LIB electrolytes, a relatively stable anionic sublattice favors migration of Na^+/Li^+ ions due to a lower activation energy (E_a) barrier and a high transference number[2,20]. However, the strong affinity of cations for the anionic sublattice leads to low ionic conductivity. Further, facile electron transfer with the anionic sublattice results in poor electronic insulation in the case of inorganic solid electrolytes, which is more suited for the design of cathode materials, though not ideal for electrolytes.

To provide higher electronic insulation and low-affinity between the cations and anionic sublattice, soft-solid co-crystals—also referred to as solvate electrolytes—for Li^+/Na^+ ion migration have been developed by the Zdilla group. Inorganic salts like LiCl, $NaClO_4$ form co-crystalline

structures with organic solvents like *N,N*-dimethylformamide (DMF), adiponitrile (ADN), and are stable at ambient temperature[21,22]. Two recent examples of such cocrystals are DMF·LiCl[21] and $(DMF)_3NaClO_4$[22]. These cocrystals exhibit moderate-to-high ionic conductivity at room temperature from 10^{-5} S-cm^{-1} to 10^{-3} S-cm^{-1} and E_a barrier to ion hopping (85 kJ-mol^{-1} and 25 kJ-mol^{-1}, respectively, from impedance spectroscopy). The advancement in the development of electrolytes is accelerated with computational methods like Molecular Dynamics (MD) simulations and density functional theory (DFT) calculations which can characterize mechanism of ion conduction[19]. Classical MD simulations are an effective method to observe ion conduction and jump events[23,24], whereas DFT-MD simulations[25] have been used to calculate more accurate barriers and structural changes during ionic diffusion. Plane-wave DFT calculations can extract minimum energy paths (MEP), electronic properties like electrochemical stability (from band structure), and defect formation enthalpies[26]. A combined approach of MD and DFT is frequently employed to extract the long-timescale diffusion and short timescale jump events[7,19]. Islam and coworkers used MD and *ab-initio* MD simulations to model the diffusive behavior in Na^+ ion electrolytes[7]. The authors extensively examined the path of Na^+ ion conduction and ascertained the migration of ions along the 1D channels to be three-dimensional in nature. Further, DFT has also been employed to calculate the minimum energy path (MEP) for ion conduction in liquid, solid, amorphous, crystalline, organic and inorganic electrolytes[18,24].

The $(DMF)_3NaClO_4$ cocrystal exhibits interesting thermomechanical behavior where it shows a first of its kind example to expel solvent from the Na^+ coordination sphere under pressure or heating. In our recent work,[27] we reported the experimental observation of stoichiometric changes (from $(DMF)_3NaClO_4$ to $(DMF)_2NaClO_4$) in these cocrystals. We further examined the mechanism of this stimuli response from classical MD simulations with effects of pressure and temperature. We also described that these crystals and others like them exhibit a nanoliquid surface layer resulting from the decreased lattice energy at the surface, which we have detected experimentally (SEM), and which we have described using MD simulations on several materials[28,29]. This surface nanoliquid layer at the grain boundaries naturally binds grains to one another and facilitates ion conduction across electrolyte particles, circumventing the grain-boundary problem common to other solid electrolyte systems. Apart from these peculiar structural properties, these cocrystals exhibit a conductivity of 3×10^{-4} S-cm^{-1} with E_a barrier of 25 kJ-mol^{-1} for Na^+ ion conduction calculated from temperature-dependent impedance spectroscopy measurements[22]. While this conductivity is excellent for a solid electrolyte, details of the ion conduction are left unresolved, since ions could conduct through several pathways: 1) through the bulk of the crystal, 2) across the grain boundary from bulk-to-bulk, or 3) along the nanoliquid surface as a percolating network. Unfortunately, the sodium ion transference number (t_{Na+}) was neither calculable from chronoamperometry due to reactivity of $(DMF)_3NaClO_4$ with Na^0 metal, nor from pulse-field gradient NMR due to fast relaxation of quadrupolar ^{11}Na nuclei.[22] Nevertheless, the presence of one-dimensional Na^+ ion channels in these structures (both stoichiometries), and the mechanism of Na^+ ion mobility are of interest in assembling foundational knowledge of ion conduction mechanisms in such materials, and are therefore ripe for theoretical investigation, and can inform the design of improved materials. With that aim, here we investigate the ionic mobilities, simulated transference numbers, jump statistics during hopping events, and the mechanism of ionic jumps for the Na^+ ions in DMF-$NaClO_4$ cocrystalline electrolytes, and compare these values to new and previously published experimental data.

Experimental and Computational Details

$(DMF)_3NaClO_4$ was prepared as previously described.[27] Electrochemical Impedance Spectroscopy (EIS) was used to measure ionic conductivities for $(DMF)_2NaClO_4$ sample from the Nyquist plots **(Figure S1)**. The Nyquist plots were extrapolated to obtain this data at different temperature using an equivalent circuit shown in **Figure S1**.

The unit cell parameters for $(DMF)_3NaClO_4$ were obtained from the single-crystal data provided by Chinnam et al.[22]. The initial benchmarks and structural validations from MD simulations were achieved using Gromacs 5.0.7[30] code with the protocols and a modified force-field discussed in our earlier work.[27] The full set of force-field parameters for $(DMF)_3NaClO_4$ are provided in the Supporting Information. A supercell with 6x6x12 unit cells (36288 atoms) of the $(DMF)_3NaClO_4$ cocrystals was used to simulate ion dynamics under *NVT* ensemble conditions with a time constant of 0.1 ps for 50 ns at various temperatures between T = 233 K and 400 K. All the simulations were carried out with a cut-off of 12 Å for the neighbor search and for the calculation of non-bonded interactions. A timestep of 1 fs was used for the integration of forces, while trajectory to analyze the dynamics of the system was recorded at every 5 ps. The first 10 ns of these trajectories were discarded and then the diffusion coefficients were calculated from Einstein's equation. Further, we have used these trajectories at various temperature and time-interval windows to analyze the jump events observed during classical simulations by calculating the self-part of van-Hove autocorrelation function[31] for Na^+ ions.

To understand the mechanism of Na^+ conduction at a more accurate level, and for the validation of jump-events obtained from classical MD trajectories, plane-wave DFT calculations were performed using the QUANTUM ESPRESSO v6.2[32,33] code. The PBE functional[34] was used with the Kresse-Joubert projector-augmented wave[35] (KJPAW) basis with a cut-off of 60 Rydberg (Ry) for the wavefunction. The convergence threshold for wavefunction was set to 10^{-7} Ry and for geometry relaxation to 10^{-3}

Ry/Bohr. A supercell of 1x1x2 (168 atoms) with a Γ-only k-mesh was used to determine MEP for $(DMF)_3NaClO_4$. A supercell of 2x1x1 (240 atoms) with a Γ-only k-mesh was used to determine MEP for $(DMF)_2NaClO_4$. The nudged elastic band (NEB) and climbing-image NEB (CI-NEB)[36] calculations were performed to calculate E_a for Na^+ conduction with 9 or more intermediate images. In order to extrapolate the MEP using NEB, reactant and product images were created by the removal of one Na^+ ion in the supercell. The obtained structures were relaxed before the NEB calculations and then several initial guesses of transition state (TS) structures were used as an intermediate image. Further, more intermediate images (up to 3) between reactant-TS and TS-product images were added and optimized under NEB to finely extrapolate the MEP.

Results and Discussion

We first examined the migration of both cations and anions in the *NVT* ensemble conditions. The MSD *vs.* time plots for Na^+ **(Figure 1a** and **1b)** and ClO_4^- **(Figure 1c** and **1d)** ions are calculated from a series of constant temperature simulations on the periodic supercell to obtain diffusion coefficients (D_i) using Einstein's equation. The MSD *vs.* time plots show that at low temperatures (T ≤ 283 K) the early diffusion of Na^+ ions is super-diffusive, due to the initial cage vibrations. However, with sufficiently long timescales (40 ns), a linearity in diffusion was observed even at low temperatures (T = 233 K to 273 K). Hence, from the linear regime of MSD *vs.* time plots, values of D_i for Na^+ and ClO_4^- were calculated for T = 233 K to T = 400 K **(Figure 2a)**. The calculated values of diffusion coefficients and transference number are provided in Table S1 of the Supporting Information.

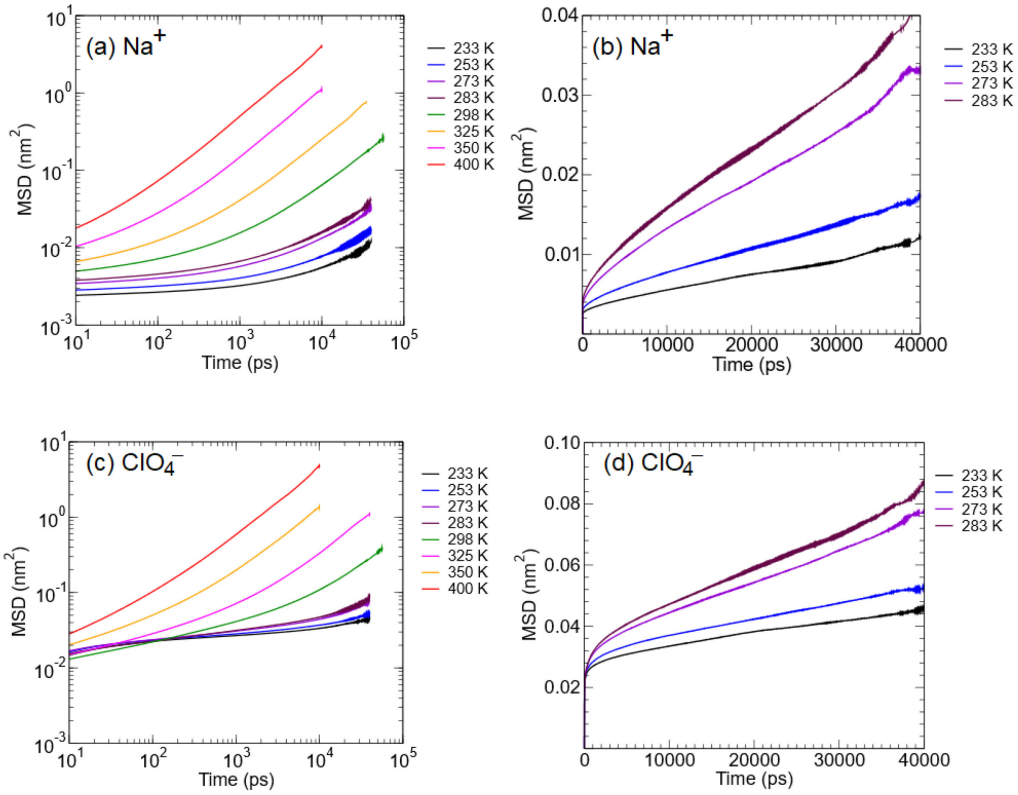

Figure 1. MSD vs. time plot for Na^+ cations on **(a)** logarithmic scale for all temperatures and **(b)** linear scale for low temperatures, and for ClO_4^- anions on **(c)** logarithmic scale for all temperatures and **(d)** linear scale for low temperatures.

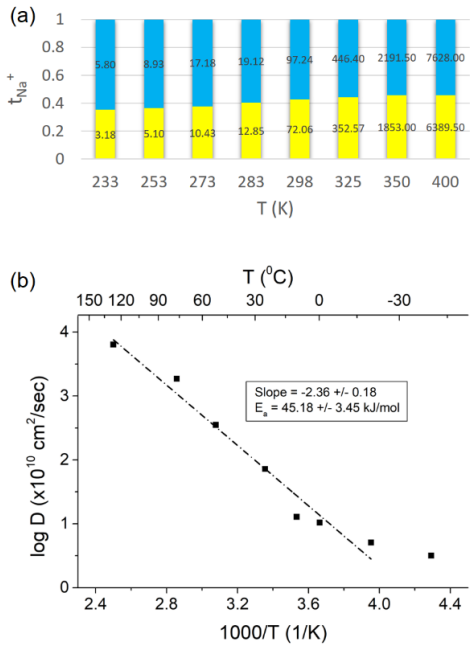

Figure 2. (a) Transference number for Na^+ ions in $(DMF)_3NaClO_4$ for various temperature values between T = 233 K and 400 K. Diffusion coefficients (10^{-10} cm²/sec) for Na^+ (yellow) and ClO_4^- (blue) calculated from simulations using Einstein's equation are provided in the respective bars, (b) log (D_{Na^+}) vs. 1/T plot from simulations for $(DMF)_3NaClO_4$, the data points were fitted to a straight line (the lowest temperature point was neglected).

In our earlier work,[27] we calculated static structure factor (radial distribution function) and histograms of cation cluster size, which showed that at low temperature (<<T_m) sodium ions remain solvated by DMF and isolated from perchlorate anions, but at high temperature (> T_m, $T_{m,exp}$ = 55 °C [22] and $T_{m,MD}$ = 52 °C [27]), the cocrystals do not phase separate, but appear as small ion-pair clusters of $NaClO_4$ solvated in DMF. This suggests that the room-temperature cocrystals behave as a superionic solution of $NaClO_4$ in DMF, and hence the calculation of D_i is relevant even at these high temperatures (T = 325 K, 350 K and 400 K). The calculated D_i values provide a t_{Na^+} = 0.43 at 298 K and demonstrate that the fraction of mobility of Na^+ ions in the net ionic mobility increases with temperature up to 0.46 at T = 400 K. The values of D_{Na^+} are fitted to Arrhenius equation to calculate E_a for Na^+ ion conduction **(Figure 2b)**. The fitted data provide an E_a barrier of 45 kJ-mol^{-1} for Na^+ ion conduction in the cocrystals, significantly higher than the $E_{a,exp}$ = 25 kJ-mol^{-1}.

To analyze the nature of Na^+ cation jump events, the self-part of VHACF was calculated for time intervals of 100 ps, 1ns and 10 ns **(Figure 3)**. VHACF shows that at low temperatures, the primary mode of Na^+ ion mobility is cage vibrations and short-distance (< 0.5 nm) jumps, whereas a few spikes associated with long-distance jumps (> 1 nm) are also observed with a small probability. As the temperature increases above room temperature, the primary peak associated with short-distance jumps decreases, indicating interstitial migration of Na^+ ions. The occurrence of longer jumps appear in wider time windows of 10 ns, due to a

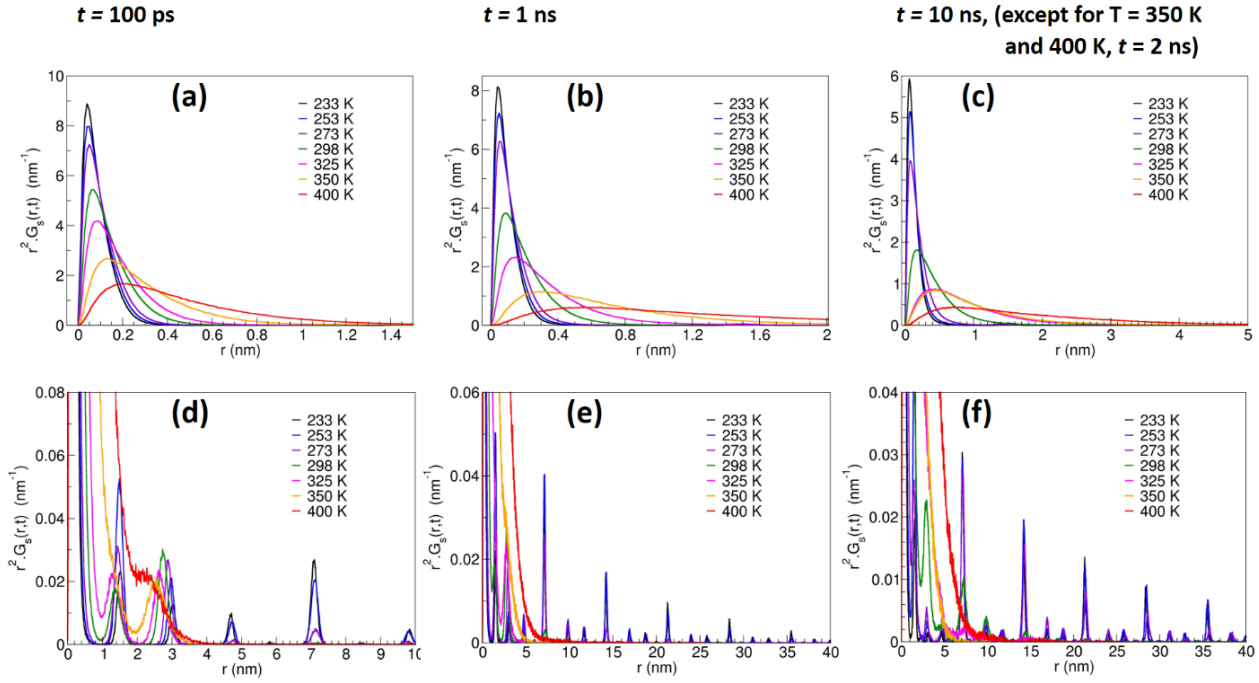

Figure 3. Self-part of van Hove ACF for Na^+ ions in $(DMF)_3NaClO_4$ at various constant temperatures and a fixed time interval from an overall trajectory of 40 ns: **(a)** t = 100 ps, **(b)** t = 1 ns, and **(c)** t = 10 ns (except for T = 350 K and 400 K, t = 2ns); **(d)**, **(e)** and **(f)** are zoomed in views on y-axis and zoomed out views on x-axis for (a), (b) and (c), respectively.

probable combination of vehicular and hopping diffusion of Na^+ ions in the crystal. The results suggest that migration through an interstitial site is likely in bulk ion conduction.

The reason behind short-distance jumps is the array of Na^+ ions with an interionic distance of 0.323 nm, as suggested from the unit cell structure obtained from single-crystal XRD. To understand these short-distance jumps, and to more rigorously estimate the energetics of this two-step process, plane-wave DFT calculations were performed to obtain the MEP for a Na^+ ion jump to the adjacent vacancy site. A 1x1x2 supercell of $(DMF)_3NaClO_4$ was created and relaxed without any restrictions of symmetry on the structure. Further, a pair of defected supercells was created with one Na^+ ion defect at an adjacent site in two supercells. The two supercell images differ only in the location of vacancy sites, are thus considered 'reactant' and 'product' geometries, indistinguishably, to optimize the MEP using NEB calculations. The extrapolated path of a Na^+ ion to migrate to a vacancy site in the *c*-crystallographic direction (at a distance of 0.323 nm) shows E_a = 0.34 eV (= 33 kJ-mol^{-1}) **(Figure 4)** closer to the experimental value of 25 kJ-mol^{-1}. The calculated E_a barrier was also validated against the energy cut-off from 40 Ry to 80 Ry (Table S2 of the Supporting Information) and the calculated E_a was found to be 0.34 ± 0.01 eV. This lower activation barrier suggests that bulk migration most likely contributes to the overall conductivity (in addition to a percolating network) due to the preponderance of bulk matter in pressed electrolyte pellets. Unlike the simulation, an interstitial site is not involved in the ion hopping pathway determined from NEB methods; the migration of a Na^+ ion occurs via formation of a trigonal planar transition state **(Supporting Movie 1)**, and represents a distinction from the higher-barrier intermediate pathway observed in the MD mechanism. The extrapolated MEP suggests that the carbonyl group on DMF molecules assists in delivering the Na^+ ion from the occupancy site to a vacancy site with a small barrier and can be termed 'solvent-assisted' migration. In the transition state, the Na^+ ion does not contact the ClO_4^-. In another work a similar solvent-assisted migration of Li^+ ion has also been observed where the cyano group on adiponitrile supports the migration of Li^+ ions to an occupancy site at a distance of > 0.6 nm, without any interference from anions.[28]

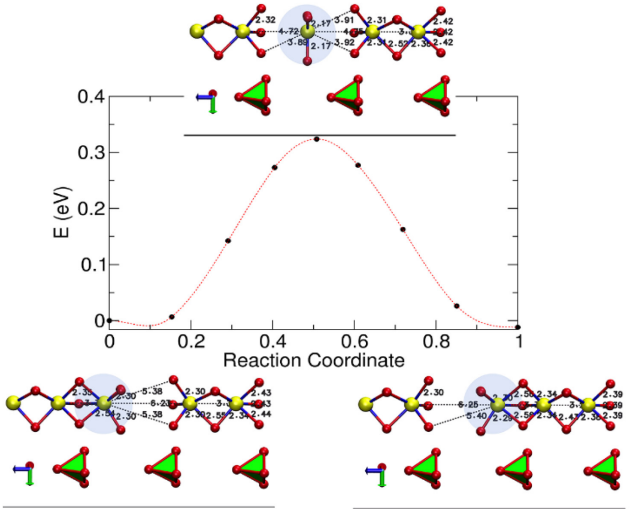

Figure 4. Minimum energy path of Na^+ ion conduction in $(DMF)_3NaClO_4$ extrapolated from NEB calculations. Color scheme: Red- O (DMF) free, red atoms in tetrahedral green cages- O in ClO_4^- anions, yellow- Na^+ ions. Distances shown as text are in the units of Å.

Despite having a close agreement for the $E_{a,exp}$ and $E_{a,DFT}$ for $(DMF)_3NaClO_4$, a poor agreement of E_a from MD simulations was still an unsolved question. We hypothesized that the MD simulations at and above room temperature do not exclusively manifest just the Na^+ ion conduction in $(DMF)_3NaClO_4$ as the simulations also have shown that around room temperature the crystals form a dynamic equilibrium with the 2:1 stoichiometry as well.[27] This has been previously reported by us from a cluster analysis with respect to a dynamic heating and constant temperature equilibrium simulations under *NVT* conditions. Also, roughly 1.8 ClO_4^- anions were seen to occupy the Na^+ solvation sphere by replacing DMF molecules in the 2:1 stoichiometry, as observed from RDF and coordination number analysis. Thus, both MSD and VHACF include a contribution from the 2:1 stoichiometric geometry as well, especially at T ≥ 298 K. Further, a higher E_a barrier than the experimental value could also be the reason for this behavior as formation of more $(DMF)_2NaClO_4$ crystal could lead to lower Na^+ ion conduction due to Na^+---ClO_4^- interactions in this stoichiometry. To test this hypothesis, we recorded impedance spectroscopy based ionic conductivities for $(DMF)_2NaClO_4$ **(Figure 5a)** and obtained a room temperature ionic conductivity to be 7 x 10^{-5} S-cm^{-1} with a calculated $E_{a,exp}$ barrier of 49 kJ-mol^{-1}. To validate this and obtain the MEP, a 2x1x1 supercell of $(DMF)_2NaClO_4$ was used to perform DFT calculations to calculate $E_{a,DFT}$ using the NEB method. Unlike in the 3:1 stoichiometry, the 2:1 cocrystal exhibits two different sites for Na^+ ions, leading to different energies for the removal of two different adjacent Na^+ ions, one each time. **Figure 5b** shows these three sites of Na^+ ions as Na_1, Na_2 and Na_3. The removal of Na_3 and Na_1 leads to similar energy configurations as the initial and final states shown in the **Figure 5c.** Removal of a Na_2 ion from

the crystal is slightly higher (0.18 eV) in energy compared with the other two, shown at the 0.5 reaction coordinate. The MEP path was extrapolated using three initial images, which included the paths between Na_1 and Na_2, and between Na_2 and Na_3. The MEP was further fine-tuned with inclusion of more images and a tighter optimization criterion where the images were considered stable only when the fluctuation was < 0.01 eV-Bohr^{-1}. The extrapolated path of Na^+ ion to migrate to a vacancy site (at a distance of 0.343 nm) shows E_a = 0.43 eV (= 41 kJ-mol^{-1}) **(Figure 5c)** close to the experimental value of 49 kJ-mol^{-1} in this stoichiometry, and closer to the value computed from the intermediate pathway seen in MD simulations. The MEP for Na^+ ion conduction in $(DMF)_2NaClO_4$ is also provided as Supporting Movie 2. These observations and those for the 3:1 geometry explain the discrepancies in the E_a barrier calculated from experiments and MD simulations: that anion-assisted sodium conduction is a high-barrier pathway, passing through a trapped ion-pair intermediate, which can, in principle, occur in both the 3:1 and the 2:1 solvates. The preferred bulk conduction pathway is directly along the crystallographic *c* axis, via a three-coordinate DMF-solvated intermediate.

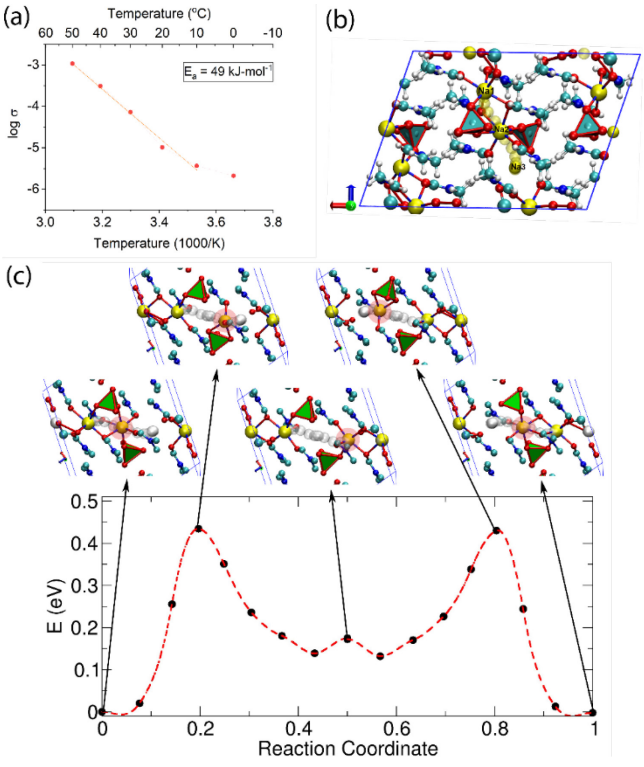

Figure 5. (a) Experimental ionic conductivity with respect to temperature for $(DMF)_2NaClO_4$ cocrystals, the straight line neglects the lowest temperature point while fitting; **(b)** A 2x1x1 supercell for $(DMF)_2NaClO_4$ crystals showing Na_1, Na_2 and Na_3 sites on the *xy*-plane. **(c)** Minimum energy path for Na^+ ion conduction in $(DMF)_2NaClO_4$ extrapolated from NEB calculations. Color scheme: Yellow solid spheres – Na^+ (actual position), White transparent spheres – Na^+ (all positions during trajectory), Red – O, Green – Cl, Cyan– C, , Blue – N.

Conclusions

In order to explain the high conductivity of $(DMF)_3NaClO_4$ and its low E_a barrier (25 kJ-mol^{-1}) using MD simulations, diffusion coefficients for cations in hard-solids would typically be calculated by performing high-temperature simulations, where cations attain linearity in diffusion and the anionic sublattice remains thermally stable (immobile). However, in soft-solid cocrystalline electrolytes, the higher stability of the cationic sublattice leaves a marginal window of temperature to observe linear diffusion. The E_a barrier for conduction of Na^+ from the Arrhenius plot (45 kJ-mol^{-1}) of diffusion coefficients, which was obtained from classical MD simulations with sufficiently long time scales, was on the same order of magnitude, but higher than the experimental value (25 kJ-mol^{-1}). The VHACF analysis of jump events shows occurrence of both short and long jump events depending upon the time-window from picoseconds to nanoseconds, respectively. The short jumps occur between the adjacent sites while the long jump events occur with a low probability in a vehicular manner as seen from the VHACF. The dissimilarity in $E_{a,exp}$ and $E_{a,MD}$ values for $(DMF)_3NaClO_4$ stoichiometry is explained by the possible involvement of an ion-paired intermediate analogous to the structure of the 2:1 stoichiometric clusters, for which $E_{a,exp}$ is 49 kJ-mol^{-1} (in agreement with $E_{a,DFT}$ = 41 kJ-mol^{-1}). The DFT calculations suggest a solvent assisted MEP for Na^+ cations (with no involvement of ClO_4^-) with a barrier of 33 kJ-mol^{-1} for $(DMF)_3NaClO_4$ crystals that is closer to the experimental value. In case of $(DMF)_2NaClO_4$, replacement of ClO_4^- anions with DMF solvent molecules, as seen in our earlier work, results in a higher barrier for Na^+ conduction compared to its 3:1 stoichiometry. Despite the use of a non-polarizable force-field for the MD simulations, the obtained diffusion coefficients and the E_a barriers for MEP are in good agreement with the experiments. The reason behind this good agreement is the inclusion of sufficient different geometries of Na^+---ClO_4^- and Na^+---DMF to calibrate the partial charges on Na^+ and $O(ClO_4^-)$ atoms.[27] Since the partial charge on the Na^+ does not change significantly during movement from one-site to another, even a non-polarizable force-field is able to capture the ion dynamics with sufficient accuracy. The probable mechanism of the high conductivity of the material is thus elucidated implicating a favorable solvent-cation coordination for better ion conduction directly between cation sites.

ASSOCIATED CONTENT

Supporting Information. Impedance spectra and equivalent circuits, force-field parameters for MD simulations, diffusion coefficients and transference numbers with respect to temperature, effect of energy cut-off on the activation energy barriers, Supporting movies illustrating mechanisms of ionic conduction, atomic coordinates from computations. This material is available free of charge via the Internet at http://pubs.acs.org.

AUTHOR INFORMATION

Corresponding Authors

* MJZ : mzdilla@temple.edu
* SLW : slwunder@temple.edu
* AV : arun@iiserpune.ac.in

Author Contributions

The manuscript was written through contributions of all authors.

ACKNOWLEDGMENT

We are grateful to DST Nanomission SR/NM/TP-13/2016, SERB DST CRG/2018/001536, IUSSTF/JC-031/2017 grants for their funding, and the National Science Foundation under award 2138432. Computational work on Temple's EFRC cluster was supported by the Center for the Computational Design of Functional Layered Materials, an Energy Frontier Research Center funded by the U.S. Department of Energy, Office of Science, Basic Energy Sciences, under Award # DESC0012575. For additional computational resources, we acknowledge Temple University's HPC resources, which were supported in part by the National Science Foundation through major research instrumentation grant number 1625061 and by the US Army Research Laboratory under contract number W911NF-16-2-0189, and National Supercomputing Mission (NSM) 'PARAM Brahma' at IISER Pune, which is implemented by C-DAC and supported by the Ministry of Electronics and Information Technology (MeitY) and Department of Science and Technology (DST), Government of India. P. P. acknowledges IISER Pune and Foreign Fulbright Program from USDOS for a graduate fellowship and a visiting research fellowship, respectively. A. S. thanks DST INSPIRE for a graduate fellowship.

REFERENCES

(1) Sun, C.; Liu, J.; Gong, Y.; Wilkinson, D. P.; Zhang, J. Recent Advances in All-Solid-State Rechargeable Lithium Batteries. *Nano Energy* **2017**, *33* (January), 363–386. https://doi.org/10.1016/j.nanoen.2017.01.028.

(2) Zhang, Z.; Shao, Y.; Lotsch, B.; Hu, Y. S.; Li, H.; Janek, J.; Nazar, L. F.; Nan, C. W.; Maier, J.; Armand, M., et al. New Horizons for Inorganic Solid State Ion Conductors. *Energy Environ. Sci.* **2018**, *11* (8), 1945–1976. https://doi.org/10.1039/c8ee01053f.

(3) Vaalma, C.; Buchholz, D.; Weil, M.; Passerini, S. A Cost and Resource Analysis of Sodium-Ion Batteries. *Nat. Rev. Mater.* **2018**, *3* (4), 18013. https://doi.org/10.1038/natrevmats.2018.13.

(4) Hess, S.; Wohlfahrt-Mehrens, M.; Wachtler, M. Flammability of Li-Ion Battery Electrolytes: Flash Point and Self-Extinguishing Time Measurements. *J. Electrochem. Soc.* **2015**, *162* (2), A3084–A3097. https://doi.org/10.1149/2.0121502jes.

(5) Manthiram, A.; Yu, X.; Wang, S. Lithium Battery Chemistries Enabled by Solid-State Electrolytes. *Nat. Rev. Mater.* **2017**, *2* (4), 1–16. https://doi.org/10.1038/natrevmats.2016.103.

(6) Anantharamulu, N.; Koteswara Rao, K.; Rambabu, G.; Vijaya Kumar, B.; Radha, V.; Vithal, M. A Wide-Ranging Review on Nasicon Type Materials. *J. Mater. Sci.* **2011**, *46* (9), 2821–2837. https://doi.org/10.1007/s10853-011-5302-5.

(7) Deng, Y.; Eames, C.; Nguyen, L. H. B.; Pecher, O.; Griffith, K. J.; Courty, M.; Fleutot, B.; Chotard, J. N.; Grey, C. P.; Islam, M. S., et al. Crystal Structures, Local Atomic Environments, and Ion Diffusion Mechanisms of Scandium-Substituted Sodium Superionic Conductor (NASICON) Solid Electrolytes. *Chem. Mater.* **2018**, *30* (8), 2618–2630. https://doi.org/10.1021/acs.chemmater.7b05237.

(8) Zhang, Z.; Zhang, Q.; Ren, C.; Luo, F.; Ma, Q.; Hu, Y.-S.; Zhou, Z.; Li, H.; Huang, X.; Chen, L. A Ceramic/Polymer Composite Solid Electrolyte for Sodium Batteries. *J. Mater. Chem. A* **2016**, *4* (41), 15823–15828. https://doi.org/10.1039/C6TA07590H.

(9) Wang, J.; Yamada, Y.; Sodeyama, K.; Watanabe, E.; Takada, K.; Tateyama, Y.; Yamada, A. Fire-Extinguishing Organic Electrolytes for Safe Batteries. *Nat. Energy* **2018**, *3* (1), 22–29. https://doi.org/10.1038/s41560-017-0033-8.

(10) Chen, C.-Y.; Kiko, T.; Hosokawa, T.; Matsumoto, K.; Nohira, T.; Hagiwara, R. Ionic Liquid Electrolytes with High Sodium Ion Fraction for High-Rate and Long-Life Sodium Secondary Batteries. *J. Power Sources* **2016**, *332*, 51–59. https://doi.org/10.1016/j.jpowsour.2016.09.099.

(11) Kim, J.-J.; Yoon, K.; Park, I.; Kang, K. Progress in the Development of Sodium-Ion Solid Electrolytes. *Small Methods* **2017**, *1* (10), 1700219. https://doi.org/10.1002/smtd.201700219.

(12) Vignarooban, K.; Kushagra, R.; Elango, A.; Badami, P.; Mellander, B. E.; Xu, X.; Tucker, T. G.; Nam, C.; Kannan, A. M. Current Trends and Future Challenges of Electrolytes for Sodium-Ion Batteries. *Int. J. Hydrogen Energy* **2016**, *41* (4), 2829–2846. https://doi.org/10.1016/j.ijhydene.2015.12.090.

(13) Hayashi, A.; Noi, K.; Sakuda, A.; Tatsumisago, M. Superionic Glass-Ceramic Electrolytes for Room-Temperature Rechargeable Sodium Batteries. *Nat. Commun.* **2012**, *3* (1), 856. https://doi.org/10.1038/ncomms1843.

(14) Zhou, C.; Bag, S.; Thangadurai, V. Engineering Materials for Progressive All-Solid-State Na Batteries. *ACS Energy Lett.* **2018**, *3* (9), 2181–2198. https://doi.org/10.1021/acsenergylett.8b00948.

(15) Wu, J. F.; Wang, Q.; Guo, X. Sodium-Ion Conduction in Na2Zn2TeO6 Solid Electrolytes. *J. Power Sources* **2018**, *402* (July), 513–518. https://doi.org/10.1016/j.jpowsour.2018.09.048.

(16) Bachman, J. C.; Muy, S.; Grimaud, A.; Chang, H.-H.; Pour, N.; Lux, S. F.; Paschos, O.; Maglia, F.; Lupart, S.; Lamp, P., et al. Inorganic Solid-State Electrolytes for Lithium Batteries: Mechanisms and Properties Governing Ion Conduction. *Chem. Rev.* **2016**, *116* (1), 140–162. https://doi.org/10.1021/acs.chemrev.5b00563.

(17) Deng, Z.; Mo, Y.; Ong, S. P. Computational Studies of Solid-State Alkali Conduction in Rechargeable Alkali-Ion Batteries. *NPG Asia Mater.* **2016**, *8* (3), e254–e254. https://doi.org/10.1038/am.2016.7.

(18) Åvall, G.; Mindemark, J.; Brandell, D.; Johansson, P. Sodium-Ion Battery Electrolytes: Modeling and Simulations. *Adv. Energy Mater.* **2018**, *8* (17), 1703036. https://doi.org/10.1002/aenm.201703036.

(19) Nolan, A. M.; Zhu, Y.; He, X.; Bai, Q.; Mo, Y. Computation-Accelerated Design of Materials and Interfaces for All-Solid-State Lithium-Ion Batteries. *Joule* **2018**, *2* (10), 2016–2046. https://doi.org/10.1016/j.joule.2018.08.017.

(20) He, X.; Zhu, Y.; Mo, Y. Origin of Fast Ion Diffusion in Super-Ionic Conductors. *Nat. Commun.* **2017**, *8* (May), 1–7. https://doi.org/10.1038/ncomms15893.

(21) Chinnam, P. R.; Clymer, R. N.; Jalil, A. A.; Wunder, S. L.; Zdilla, M. J. Bulk-Phase Ion Conduction in Cocrystalline LiCl·*N,N*-Dimethylformamide: A New Paradigm for Solid

Electrolytes Based upon the Pearson Hard–Soft Acid–Base Concept. *Chem. Mater.* **2015**, *27* (16), 5479–5482. https://doi.org/10.1021/acs.chemmater.5b00940.

(22) Chinnam, P. R.; Fall, B.; Dikin, D. A.; Jalil, A.; Hamilton, C. R.; Wunder, S. L.; Zdilla, M. J. A Self-Binding, Melt-Castable, Crystalline Organic Electrolyte for Sodium Ion Conduction. *Angew. Chemie Int. Ed.* **2016**, *55* (49), 15254–15257. https://doi.org/10.1002/anie.201606363.

(23) Wood, S. M.; Eames, C.; Kendrick, E.; Islam, M. S. Sodium Ion Diffusion and Voltage Trends in Phosphates $Na_4M_3(PO_4)_2P_2O_7$ (M = Fe, Mn, Co, Ni) for Possible High-Rate Cathodes. *J. Phys. Chem. C* **2015**, *119* (28), 15935–15941. https://doi.org/10.1021/acs.jpcc.5b04648.

(24) Dawson, J. A.; Chen, H.; Islam, M. S. Composition Screening of Lithium- and Sodium-Rich Anti-Perovskites for Fast-Conducting Solid Electrolytes. *J. Phys. Chem. C* **2018**, *122* (42), 23978–23984. https://doi.org/10.1021/acs.jpcc.8b08208.

(25) de Klerk, N. J. J.; van der Maas, E.; Wagemaker, M. Analysis of Diffusion in Solid-State Electrolytes through MD Simulations, Improvement of the Li-Ion Conductivity in β-Li 3 PS 4 as an Example. *ACS Appl. Energy Mater.* **2018**, *1* (7), 3230–3242. https://doi.org/10.1021/acsaem.8b00457.

(26) Urban, A.; Seo, D.-H.; Ceder, G. Computational Understanding of Li-Ion Batteries. *npj Comput. Mater.* **2016**, *2* (January), 16002. https://doi.org/10.1038/npjcompumats.2016.2.

(27) Prakash, P.; Ardhra, S.; Fall, B.; Zdilla, M. J.; Wunder, S. L.; Venkatnathan, A. Solvate Sponge Crystals of (DMF) 3 NaClO 4 : Reversible Pressure/Temperature Controlled Juicing in a Melt/Press-Castable Sodium-Ion Conductor. *Chem. Sci.* **2021**, *12* (15), 5574–5581. https://doi.org/10.1039/D0SC06455F.

(28) Fall, B.; Prakash, P.; Aguirre, J.; Chereddy, S.; Chinnam, P. R.; Dikin, D.; Venkatnathan, A.; Wunder, S. L.; Zdilla, M. J. A Soft-Solid Co-Crystalline Electrolyte Combining Advantages of Organics and Ceramics: Thermally, Electrochemically Stable, Highly Conductive (Adiponitrile)2LiPF6. *ChemRxiv* **2021**. https://doi.org/10.33774/chemrxiv-2021-nod4x.

(29) Fall, B.; Prakash, P.; Gau, M. R.; Wunder, S. L.; Venkatnathan, A.; Zdilla, M. J. Experimental and Theoretical Investigation of the Ion Conduction Mechanism of Tris(Adiponitrile)Perchloratosodium, a Self-Binding, Melt-Castable Crystalline Sodium Electrolyte. *Chem. Mater.* **2019**, *31* (21), 8850–8863. https://doi.org/10.1021/acs.chemmater.9b02853.

(30) Abraham, M. J.; Murtola, T.; Schulz, R.; Pall, S.; Smith, J. C.; Hess, B.; Lindah, E. Gromacs: High Performance Molecular Simulations through Multi-Level Parallelism from Laptops to Supercomputers. *SoftwareX* **2015**, *1–2*, 19–25. https://doi.org/10.1016/j.softx.2015.06.001.

(31) Van Hove, L. Correlations in Space and Time and Born Approximation Scattering in Systems of Interacting Particles. *Phys. Rev.* **1954**, *95* (1), 249–262. https://doi.org/10.1103/PhysRev.95.249.

(32) Giannozzi, P.; Baroni, S.; Bonini, N.; Calandra, M.; Car, R.; Cavazzoni, C.; Ceresoli, D.; Chiarotti, G. L.; Cococcioni, M.; Dabo, I., et al. QUANTUM ESPRESSO: A Modular and Open-Source Software Project for Quantum Simulations of Materials. *J. Phys. Condens. Matter* **2009**, *21* (39), 395502. https://doi.org/10.1088/0953-8984/21/39/395502.

(33) Giannozzi, P.; Andreussi, O.; Brumme, T.; Bunau, O.; Buongiorno Nardelli, M.; Calandra, M.; Car, R.; Cavazzoni, C.; Ceresoli, D.; Cococcioni, M., et al. Advanced Capabilities for Materials Modelling with Quantum ESPRESSO. *J. Phys. Condens. Matter* **2017**, *29* (46), 465901. https://doi.org/10.1088/1361-648X/aa8f79.

(34) Perdew, J. P.; Ernzerhof, M.; Burke, K. Rationale for Mixing Exact Exchange with Density Functional Approximations. *J. Chem. Phys.* **1996**, *105* (22), 9982–9985. https://doi.org/10.1063/1.472933.

(35) Kresse, G.; Joubert, D. From Ultrasoft Pseudopotentials to the Projector Augmented-Wave Method. *Phys. Rev. B* **1999**, *59* (3), 1758–1775. https://doi.org/10.1103/PhysRevB.59.1758.

(36) Henkelman, G.; Uberuaga, B. P.; Jónsson, H. A Climbing Image Nudged Elastic Band Method for Finding Saddle Points and Minimum Energy Paths. *J. Chem. Phys.* **2000**, *113* (22), 9901–9904. https://doi.org/10.1063/1.1329672.

TOC Graphic